Generation of kinetic Alfven waves in the high-latitude near-Earth magnetotail: A global hybrid simulation

Zhifang Guo, Minghua Hong, Yu Lin, Aimin Du, Xueyi Wang, Mingyu Wu, and Quanming Lu

---

Articles you may be interested in

The temporal evolution of the kinetic drift-Alfven instability of plasma shear flow
Phys. Plasmas **21**, 032118 (2014); 10.1063/1.4869094

Drift-Alfven waves induced optical emission fluctuations in Aditya tokamak
Phys. Plasmas **17**, 072515 (2010); 10.1063/1.3461165

Kinetic electron closures for electromagnetic simulation of drift and shear-Alfvén waves. II
Phys. Plasmas **9**, 1915 (2002); 10.1063/1.1454999

Kinetic electron closures for electromagnetic simulation of drift and shear-Alfvén waves. I.
Phys. Plasmas **9**, 251 (2002); 10.1063/1.1428759

Zonal flow and field generation by finite beta drift waves and kinetic drift-Alfvén waves
Phys. Plasmas **8**, 3907 (2001); 10.1063/1.1386640

Generation of kinetic Alfven waves in the high-latitude near-Earth magnetotail: A global hybrid simulation

Zhifang Guo,[1,2,3] Minghua Hong,[1,2] Yu Lin,[4,5] Aimin Du,[1,2] Xueyi Wang,[4,5] Mingyu Wu,[4,6] and Quanming Lu[4,6,a)]

[1]*Key Laboratory of Ionospheric Environment, Institute of Geology and Geophysics, Chinese Academy of Sciences, Beijing 100029, China*
[2]*Beijing National Observatory of Space Environment, Institute of Geology and Geophysics, Chinese Academy of Sciences, Beijing 100029, China*
[3]*University of Chinese Academy of Sciences, Beijing 100049, China*
[4]*CAS Key Lab of Geoscience Environment, Department of Geophysics and Planetary Science, University of Science and Technology of China, Hefei 230026, China*
[5]*Physics Department, Auburn University, 206 Allison Laboratory, Auburn, Alabama 36849-5311, USA*
[6]*Collaborative Innovation Center of Astronautical Science and Technology, China*

In this paper, effects of a fast flow in the tail plasma sheet on the generation of kinetic Alfven waves (KAWs) in the high-latitude of the near-Earth magnetotail are investigated by performing a two-dimensional (2-D) global-scale hybrid simulation, where the plasma flow is initialized by the $\mathbf{E} \times \mathbf{B}$ drift near the equatorial plane due to the existence of the dawn-dusk convection electric field. It is found that firstly, the plasma sheet becomes thinned and the dipolarization of magnetic field appears around $(x, z) = (-10.5R_E, 0.3R_E)$, where R_E is the radius of the Earth. Then, shear Alfven waves are excited in the plasma sheet, and the strong earthward flow is braked by the dipole-like magnetic field. These waves propagate along the magnetic field lines toward the polar regions later. Subsequently, KAWs with $k_\perp \gg k_\parallel$ are generated in the high-latitude magnetotail due to the existence of the non-uniformity of the magnetic field and density in the polar regions. The ratio of the electric field to the magnetic field in these waves is found to obey the relation $(\delta E_z)/(\delta B_y) \sim \omega/k_\parallel$ of KAWs. Our simulation provides a mechanism for the generation of the observed low-frequency shear Alfven waves in the plasma sheet and kinetic Alfven waves in the high-latitude near-Earth magnetotail, whose source is suggested to be the flow braking in the low-latitude plasma sheet. © 2015 AIP Publishing LLC. [http://dx.doi.org/10.1063/1.4907666]

I. INTRODUCTION

Kinetic Alfven waves (KAWs) are the shear Alfven mode in the short wavelength and dispersive regime. Their perpendicular wavelengths are comparable to either the ion gyroradius or the electron inertial length, while parallel wavelengths are longer than the ion inertial length (here, the parallel and perpendicular directions are relative to the local magnetic field).[1–3] KAWs carry a parallel electric field, and their frequencies are below or comparable to the ion cyclotron frequency.[2,4] Due to the existence of the parallel electric field and small perpendicular wavelengths, KAWs can lead to the acceleration and heating of charged particles along the magnetic field,[3,5–10] the breaking of the motion constants and consequently the cross-field particle transport.[11–14] In the Earth's magnetosphere, KAWs have been suggested to provide a possible mechanism for auroral electron acceleration in the high-latitude magnetotail.[2,4,15,16]

The existence of KAWs in the high latitude of the magnetotail has been evidenced.[17–19] Based on the measurements from the Polar spacecraft, Wygant *et al.*[17] found that the observed waves in the high-latitude magnetotail have a large characteristic amplitude ratio of the electric to magnetic field

fluctuations. They indicated that the observed waves are KAWs with perpendicular scale sizes comparable to the ion gyroradius. Besides the large ratio between the amplitudes of electric and magnetic field fluctuations, Dombeck *et al.*[18] confirmed that the frequency characteristics of these waves are also consistent with those of KAWs.

It has been suggested that KAWs can be generated through mode conversion,[1,5,20–22] phase mixing,[6,23,24] resonant absorption,[11,25] velocity shear,[26,27] etc. Hasegawa[1] proposed that MHD surface waves could couple to KAWs via an interaction with the density gradient at the plasma sheet–tail lobe boundary. Lee *et al.*[11] proposed that field line resonances may be the dominant generation process of KAWs. Hasegawa and Chen[6] also showed that KAWs can be generated by spatial phase mixing. Jaun *et al.*[28] presented a new kinetic Alfven mode conversion mechanism through a toroidal coupling. Previous studies also suggested the generation of KAWs by a velocity shear in a plasma boundary.[26,27] Additionally, Hong, Lin and Wang[29] proposed a new mechanism of the generation of kinetic Alfven waves using a two-dimensional hybrid simulation: the KAWs are generated by ion beam-plasma interaction in a non-uniform plasma boundary layer. All evidences showed that generation of KAWs is associated with a non-uniform background plasma and magnetic field, such as density, pressure, and magnetic field gradients.

a)Author to whom correspondence should be addressed. Electronic mail: qmlu@ustc.edu.cn

22, 022117-1

Nevertheless, the generation of KAWs in the high-latitude magnetotail of the Earth's magnetosphere is still not understood. Wygant *et al.*[17] provided the first evidence for small-scale kinetic Alfven waves in the high-latitude magnetotail during the onset time and expansion phase of substorms. Meanwhile, they proposed that KAWs in the high-latitude magnetotail are originated from the low-frequency Alfven waves in the low-latitude magnetotail. Space observations suggested that Alfven waves in the low-latitude magnetotail are associated with earthward fast flows produced during substroms.[30–32] The earthward fast flow is closely related to the formation of the magnetic dipolarization.[33] The dipolarization often appears in the near-Earth magnetotail during substorms.[34–37] Sergeev *et al.*[38] studied the propagation of the wide fast flow jet origin from about $40R_E$ in the midtail, and found that the jet is able to reach the inner magnetosphere at $6.6R_E$ in about 10 min. This property conforms to the results of previous MHD simulations on the basis of the spontaneous fast reconnection model.[39] When the fast flow reaches the near-Earth magnetotail, it is obstructed, which is in good agreement with the observation results of earthward fast flows.[40]

Hybrid simulations have been widely used to investigate the kinetic physics of magnetic reconnection, substorm, low-frequency waves, and associated ion dynamics. Hesse, Winske, and Kuznetsova[41] presented hybrid simulation results of collisionless magnetic reconnection in a current sheet with a normal component of the magnetic field and width of an ion inertial length. Krauss-Varban and Omidi[42] used 2-D hybrid simulations to investigate ion kinetic physics associated with the quasi-steady reconnection in the magnetotail. 2-D hybrid simulations were also carried out to study the structure of the reconnection layer in the distant magnetotail.[43] Karimabadi *et al.*[44] used both two- and three-dimensional hybrid models to investigate magnetic reconnection in a current sheet within ion gyroradius. On the other hand, Lin and Swift[45] studied the evolution of the near-Earth plasma sheet by a global 2-D hybrid model. The substorm onset and generation of field-aligned currents in the plasma sheet were also simulated by Swift and Lin.[46] Furthermore, the 2-D global hybrid model was used by Hong, Swift, and Lin[47] to study the ion dynamics associated with Alfven waves in the near-Earth magnetotail. Recently, Lin, Johnson, and Wang[21,22] investigated the mode conversion and structure of KAWs around the magnetopause boundary layer with both 2-D and 3-D hybrid simulations. Meanwhile, the generation of KAWs in the global magnetotail has not been addressed, although a 2-D hybrid simulation has already been utilized to investigate the generation of KAWs in a non-uniform magnetospheric plasma boundary layer.[29]

In this paper, by using a 2-D global hybrid simulation, we investigate the effects of the fast flow on the generation of Alfven waves in the near-Earth magnetotail, where the plasma flow is initialized by the $E \times B$ drift due to the existence of the dawn-dusk convection electric field. It is shown that shear Alfven waves are originated in the low-latitude magnetotail as a result of the fast flow, and KAWs are then produced in the high-latitude magnetotail during the poleward propagation of the shear Alfven waves along the

magnetic field lines. A possible mechanism is given for the generation of KAWs observed in the high-latitude magnetotail of the near-Earth. It is noted that the convection of resulting waves in the dawn-dusk direction is ignored in the 2-D hybrid simulation model, and the 2-D simulation may have also exaggerated the pileup of plasma in the near-Earth region due to the earthward flow.

The outline of the paper is as follows. The simulation model is described in Sec. II. The simulation results are presented in Sec. III. A summary and discussion is given in Sec. IV.

II. SIMULATION MODEL

A 2-D global-scale hybrid simulation is performed in this paper. In the hybrid model, the ions (protons) are treated as discrete, fully kinetic particles, and the electrons are assumed to be a massless fluid. The details of the simulation model have been described by Swift and Lin.[46] The simulation is performed in the noon-midnight meridian plane of the Earth's magnetosphere, and the simulation domain includes the plasma sheet and magnetotail lobes. A generalized curvilinear coordinate system, with 121×181 coordinate grids, is used in the simulation. One of the coordinate boundaries is the surface of the Earth at the geocentric distance of $1R_E$. Two other boundaries are the polar axes, which extend out to $\pm 12R_E$, and the outer boundary that extends to the radial distance of $x = -36R_E$ in the tail. The coordinate system is specified as a table giving the GSM coordinate of the coordinate points, in which x is in the sunward direction, y in the dawn-dusk direction, and z aligned along the magnetic polar axes. Only the nightside ($x < 0$) is included in the calculation.

Initially, the magnetic field consists of a 2-D dipole field plus a tail-like field, which corresponds to a current sheet with a half-width of $0.5R_E$. The current in the sheet is directed along the y direction, and the normal of the sheet is along the z direction. The dipole field strength on the Earth's surface is $50 \, \text{s}^{-1}$, corresponding to the gyrofrequency of a 5 AUM ion in a 2500 nT field, close to the geometric mean of the H^+ and O^+ masses. This particular field scaling is chosen so that the nominal tail field would scale to 15 nT, comparable to the observed values. The B_y component normal to the plane of the simulation is initially set to zero. The initial ion particle density contains two populations. A cold population has a thermal velocity of 101 km/s, filling the lobe region of the magnetotail and the semicircular region surrounding the earth within about $6R_E$. A hot population occupies the plasma sheet with a half-width of $0.5R_E$ in the z direction and in $x < -6R_E$, with a thermal velocity of 304 km/s. The initial density in the lobe is uniform and has a value of $400/R_E^3$, which gives a lobe Alfven velocity of 676 km/s. This density is adjusted to maintain the initial stress balance with the tail-like field in the z direction. A total of 3.2×10^6 particles are initially loaded. Additionally, the region from $6R_E$ inward is filled with a cold fluid in an MHD approximation. The transition region between the kinetic and fluid populations has a scale thickness of $0.6R_E$. The plasma flow is initialized according to the $E \times B$ drift due to the dawn-dusk

convection electric field of $E_y = 2.3 \text{mV/m}$, corresponding to the generated by the solar wind with a speed of 400km/s carrying a 5 nT field.

For the boundary fields at the Earth's surface and on the outer boundary, the tangential components of the electric field and the normal component of the magnetic field are specified. The radial component of the magnetic field at the Earth's surface is assumed to be fixed to its dipole value. For the run that is featured in this paper, the constant dawn-dusk electric field $E_{y0} = 2.3 \text{mV/m}$. This field is implemented along the entire boundaries, except that the tangential electric field is taken to be zero at the Earth's surface.

In the simulation, the density is expressed in units of the ion number density N_0 in the lobe, and the magnetic field is in units of the asymptotic lobe field, B_0. The time t is expressed in units of second, and the distances are measured in Earth radius, R_E. The velocity is in units of the lobe Alfven speed, V_{A0}.

III. SIMULATION RESULTS

Figure 1 presents the contour plots of the y-component the magnetic field B_y, ion density N, and the earthward ion flows V_x in a time sequence of $t = 0.0, 22.0, 27.0, 36.0,$ and 44.0. Superposed on the ion density plots are the magnetic field lines. The arrows in the right panel show the ion flow vectors, while the white dashed lines mark the position $x = -10R_E$. Initially, the dawn-dusk magnetic field component $B_y = 0$, and the simulation domain contains a high density dipole field region, low density lobes, and a density peak in the plasma sheet, where the high-speed initial earthward flow exists. In $t > 0$, the tail current sheet first undergoes a thinning process due to the unbalanced stress in the x direction, as described by Swift and Lin.[46] Small perturbations in B_y and the ion density gradually develop. At $t = 22.0$, the disturbance can be seen around $(x,z) = (-10.0, 0.0)R_E$ in the low-latitude of the near-Earth magnetotail, as well as in the plasma sheet boundaries. Dipolarization of the tail magnetic field can be seen at $t = 27.0$. Here, the dipolarization is defined as the turning of the local magnetic field direction from a nearly radial to a more north-south orientation. In the stage of the dipolarization, considerable variations of B_y appear in the low-latitude magnetotail around $(x,z) = (-10.0, 0.0)R_E$. They then develop into field-aligned structures and propagate toward the high-latitudes along the field lines. It is probable that fluctuations in the ion density are associated with these field-aligned structures. The dipolarization at $t = 27.0$ is associated with the constant accumulation of earthward moving plasmas around $(x,z) = (-10.0, 0.0)R_E$ and the subsequent tailward expansion of the field due to the enhanced total pressure. At $t = 36.0$, the region of perturbations in B_y and N in the dipole-like field has expanded poleward and tailward. At $t = 44.0$, large perturbations of N and B_y still exist in the high-latitude magnetotail, and the wave structure has developed into fine field-aligned structures with a small perpendicular wavelength. The perturbations in B_y and N continuously propagate poleward and expand tailward in the low-latitude of the magnetotail.

Our results show that when the fast earthward flow reaches around $x = -10R_E$ in the low-latitude magnetotail, it is braked by the strong dipole field. The detailed description of this process is illustrated in the right panel of Figure 1. Initially, the plasma flow is determined by the drift due to the dawn-dusk convection electric field. At $t = 22.0$, the north-south width of the strong earthward ion flow region is about $3R_E$. The brake of the earthward flow appears at about $x = -10R_E$. From t = 22.0 to 44.0, the brake zone, where the earthward flow stagnates, is seen to retreat from $x = -10R_E$ to $-13.6R_E$ in the near-Earth magnetotail. The turning-back flow direction indicates the rebound of the plasma by the dipole field, as shown at $t = 27.0, 36.0,$ and 44.0 near the brake zone, which is consistent with the observations of Du *et al.*[48]

The ion flow arrows show a significant, sharp northward and southward diversion of the flow. Figure 2(a) depicts the time evolution of B_z and B_x at $(x,z) = (-10.5, 0.3)R_E$, and the vertical dashed line indicating $t = 22.0$. Before about $t = 22.0$, the plasma sheet becomes thinned, which can be identified by the increase of B_x and the decrease of B_z at $(x,z) = (-10.5, 0.3)R_E$. After $t = 22.0$, with the brake of the earthward flow by the dipole field, B_x decreases and B_z increases at $(x,z) = (-10.5, 0.3)R_E$, and the dipolarization appears. Such a process has also been found previously by Swift and Lin.[46] Figure 2(b) illustrates the spatial profile of the ion flow V_x along x direction at $z = 0.3R_E$ during the time interval $t = 0 - 60$. The abrupt decrease of V_x from $V_x = 0.9$ to $V_x \sim 0$, e.g., near $x = -10.0R_E$ at $t = 22.0$, indicates the flow braking point and thus the dipolarization front, which moves tailward with time. The tail side of the dipolarization front is also demonstrated in this plot. At about t = 44.0, the ion flow V_x becomes tailward at $(x,z) = (-10.5, 0.3)R_E$, which leads to the increase of B_x and decrease of B_z at $t = 44.0$ in Figure 2(a).

During the above dynamic processes of the magnetotail, wave perturbations are found throughout the plasma sheet and the dipole-like magnetospheric regions. Furthermore, waves of the low-latitude and high-latitude regions exhibit different structural properties. As shown in Figure 1, large-scale fluctuations are generated in the low-latitude magnetotail during the dipolarization process. Such waves propagate to the high-latitude ionosphere along the magnetic field lines. During the propagation of the large-scale fluctuations, small-scale fluctuations are found to be generated in the high-latitude magnetotail around $7R_E$, where the plasma density and magnetic field show strong turbulence. In order to illustrate the detailed wave properties, we choose a low-latitude region around $(x,z) = (-10.0, 0.0)R_E$ and a high-latitude region around $(x,z) = (-5.0, 5.0)R_E$ for analysis. Three boxes are selected for these two regions, as marked in Figure 1, with the box denoted by "a" in the low-latitude magnetotail just above the equator (from $x = -10.0R_E$ to $-11.5R_E$ and $z = 0.0R_E$ to $2R_E$), the box denoted by "b" in the low-latitude region just at the equator (from $x = -10.0R_E$ to $-11.5R_E$ and $z = -2.0R_E$ to $2R_E$), and the one denoted by "c" in the high-latitude dipole-like region of the northern hemisphere (from $x = -4.0R_E$ to $-6R_E$ and $z = 4.0R_E$ to $5.5R_E$), as marked in Figure 1.
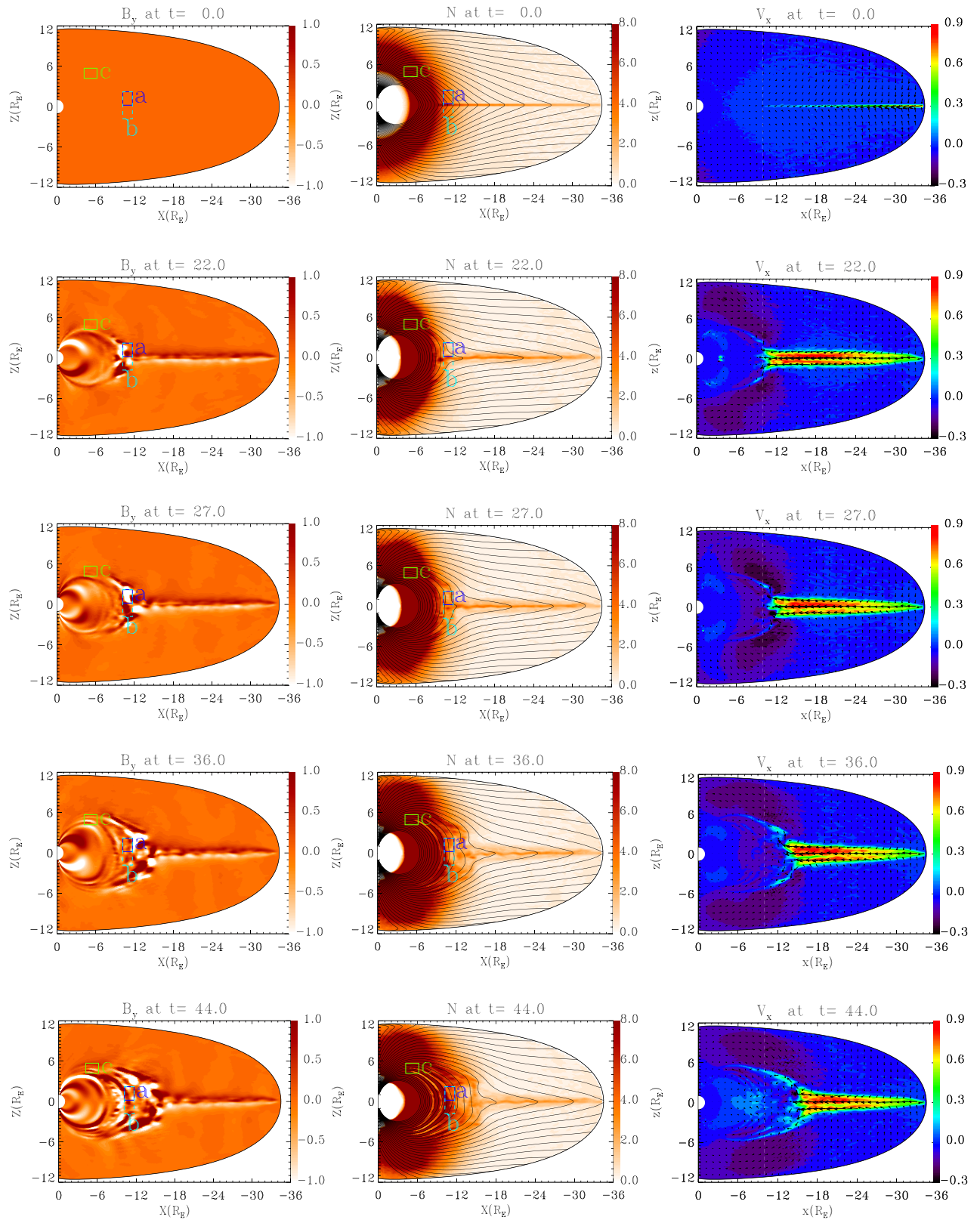
FIG. 1. Contour plots of the y-component magnetic field B_y, the ion density N, and the earthward ion flows V_x in a time sequence of $t = 0.0, 22.0, 27.0, 36.0,$ and 44.0. Superposed on the ion density plots are the magnetic field lines. Box "a" (from $x = -10R_E$ to $-11.5R_E$ and $z = 0.0R_E$ to $2R_E$) and box "b" (from $x = -10R_E$ to $-11.5R_E$ and $z = -2.0R_E$ to $2R_E$) are in the low-latitude magnetotail and box "c" (from $x = -4.0R_E$ to $-6.0R_E$ and $z = 4.0R_E$ to $5.5R_E$) is in the high-latitude region of the northern hemisphere. The arrows in the right panel show the ion flow vectors, while the white dashed lines show the position $x = -10R_E$.

To illustrate the wave modes for the fluctuations in the low-latitude magnetotail, Figures 3(a) and 3(b) show, in turn, the $\omega - k_\parallel$ dispersion relation of the waves in the regions denoted by "a" and "b." At these two locations, k_z is approximately the parallel wave number $k_\parallel$. The dispersion relation is calculated during the interval from $t = 20.0$ to
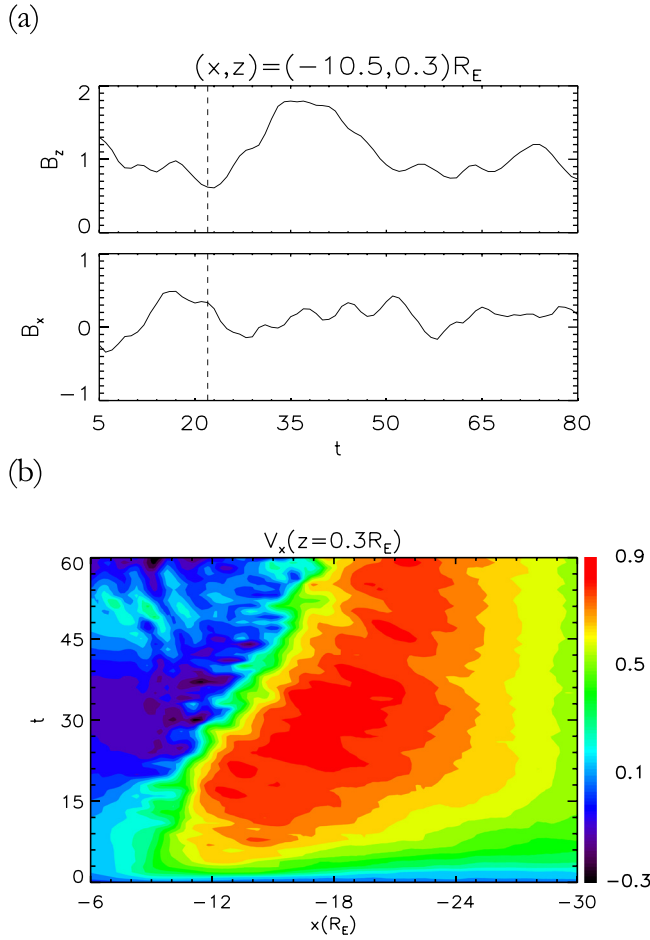
(a)

(b)

FIG. 2. (a) Time evolution of B_z and B_x at $(x,z) = (-10.5, 0.3)R_E$, with the vertical dashed line indicating $t = 22.0$. (b) Time evolution of the spatial profile of V_x along the x direction at $z = 0.3R_E$ in a time sequence from $t = 0 - 60.0$.

$t = 40.0$. In Figure 3, the solid line depicts the dispersion relation for shear Alfven waves, i.e., $\omega = k_\parallel V_A$, with V_A being the local Alfven speed, while the dashed line shows the fitted value based on the simulation data. It can be seen from Figure 3(a) that the waves in region "a," above the equator, satisfy the shear Alfven wave dispersion relation $\omega = k_\parallel V_A$, with wave propagation direction $k_z > 0$, to the north. The wave polarization is found to be dominated by the shear components B_y, further indicating the existence of shear Alfven waves. In region "b" centered at the equator, the waves are also shear Alfven waves, but wave modes with both $k_z > 0$ and $k_z < 0$ are identified, as seen in Figure 3(b). It demonstrates the propagation of Alfven waves from the equatorial magnetotail plasma sheet ($z \simeq 0$) to the northern and southern polar regions along the magnetic field lines.

As these Alfven waves propagate in the near-Earth dipole magnetosphere, they develop into small-scale structures with a dominant wave number in the direction perpendicular to the magnetic field. To illustrate the detailed characteristics of the small-scale fluctuations generated in the magnetosphere, we now analyze the waves in region "c" around $(x,z) = (-5.0, 5.0)R_E$, as marked in Figure 1. It is noted that the magnetic field is almost parallel to the x direction around this high-latitude region. The waves have a large
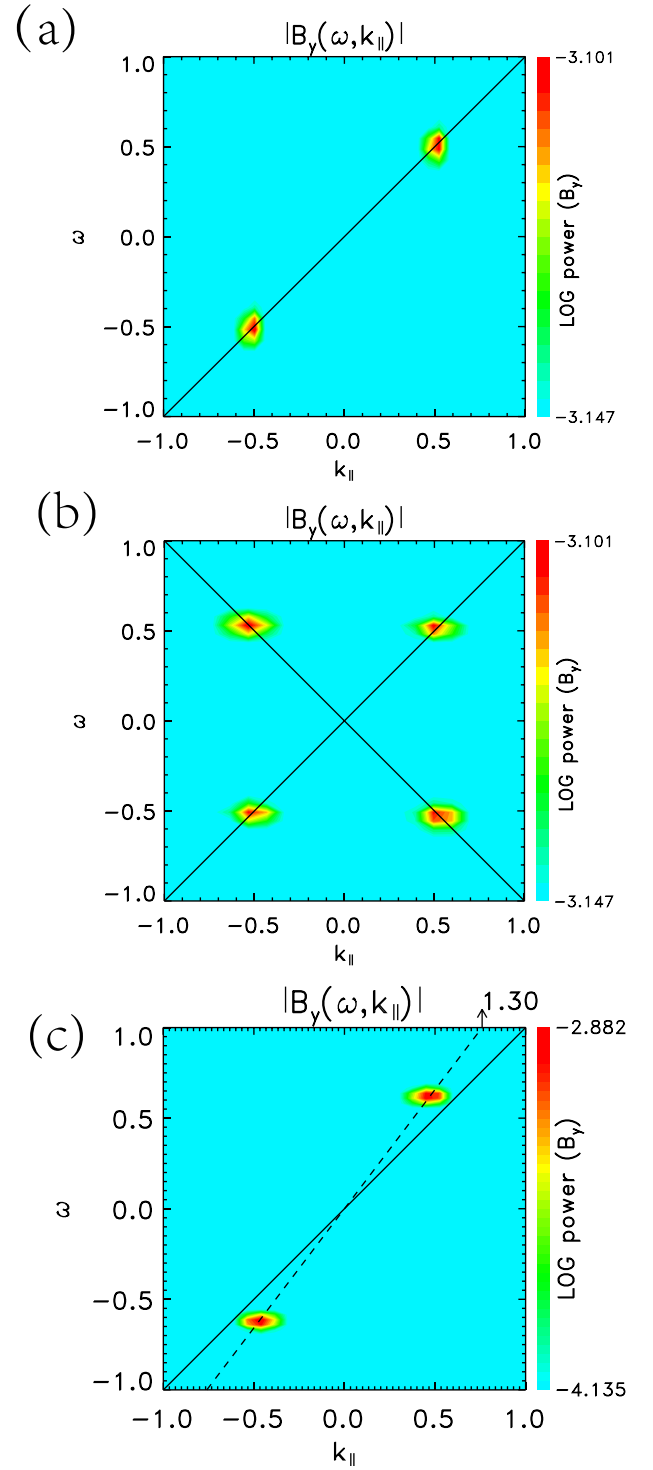
(a)

(b)

(c)

FIG. 3. (a)–(c) Dispersion relation $\omega - k_\parallel$ based on the Fourier transform of waves in the regions denoted by "a," "b," and "c" as marked in Figure 1, respectively. The solid line depicts the shear Alfven dispersion relation $\omega = k_\parallel V_A$, with V_A being the local Alfven speed. The dashed line shows the fitted value based on the simulation data.

parallel wavelength as can be seen in Figure 1. The dominant wave vectors are found to be approximately in the z direction, perpendicular to the magnetic field ($k_\perp \gg k_\parallel$). Figure 4(a) shows the spatial cuts of the magnetic field B, B_y and the ion density N from $z = -10R_E$ to $z = 10R_E$ along $x = -5.0R_E$ at $t = 36.0$. The field component B_y and the ion density N display coherent wave structures around $z = \pm 5R_E$,
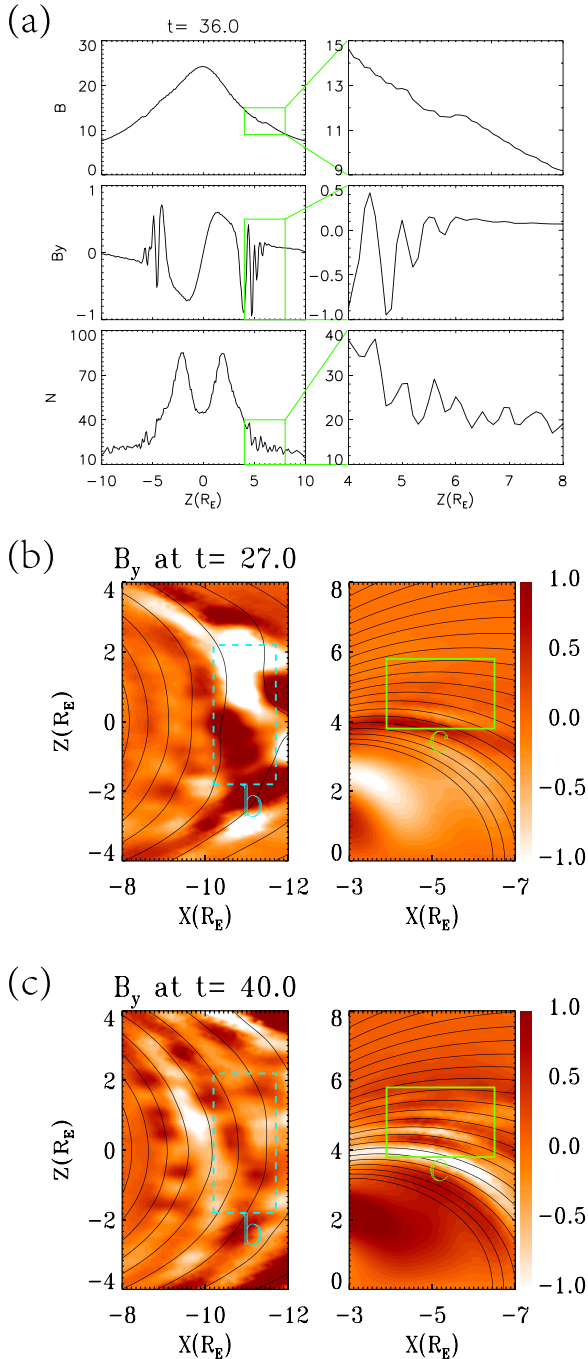
FIG. 4. (a) Spatial cuts of total magnetic field B, B_y and the ion density N from $z = -10R_E$ to $10R_E$ along $x = -5R_E$ at $t = 36.0$. The right panel depicts the spatial cuts of B, B_y and the ion density N along z at $x = -5R_E$ from $z = 4R_E$ to $8R_E$, respectively. (b) The enlarged images of B_y in regions "b" and "c" at $t = 27.0$. (c) The enlarged images of B_y in regions "b" and "c" at $t = 44.0$. Superposed on the magnetic field B_y plots are the magnetic field lines.

with the perpendicular wavelength $\lambda_\perp \sim 0.34 - 0.67R_E$, which corresponds to $k_\perp \rho_i \sim 0.33 - 0.65$, where ρ_i is the local Larmor radius. In the regions with coherent wave structures in Figure 4(a) (the region in $z > 0$ coincides with region "c" in Figure 1), the magnetic field B_y and the ion density are non-uniform. Previous studies[49,50] have shown KAWs can be excited in the region with an inhomogeneous plasma density and magnetic field. Figures 4(b) and 4(c)

show the enlarged images of B_y in regions "b" and "c" at times $t = 27.0$ and 44.0, respectively. Superposed on the magnetic field B_y plots are the magnetic field lines. At $t = 27.0$, large-amplitude magnetic fluctuations can be observed in region "b," and the field-aligned structures are gradually formed. Later at $t = 44.0$, the disturbance still exists in region "b," while field-aligned structures with large variation perpendicular to the magnetic field appear in region "c," and its short perpendicular wavelength corresponding to $k_\perp \rho_i \sim 0.33 - 0.65$. In the present simulation, the fluctuations in region "c" are also identified as kinetic Alfven waves. Figure 3(c) shows the dispersion relation for region "c" obtained from the simulation from t = 20.0 to 40.0, which is fitted as $\omega = 1.30k_\parallel V_A$, consistent with the theoretically predicted $\omega \sim 1.20k_\parallel V_A$ on the basis of the analytical KAWs dispersion relation $\omega^2 = k_\parallel^2 V_A^2 [1 + (1 + \frac{T_e}{T_i})k_\perp^2 \rho_i^2]$.

For the waves in region "c," Figure 5(a) shows the time evolution of the magnetic field B_y (red line) and the electric field E_z (black line) at $(x, z) = (-5.0, 5.0)R_E$, and Figure 5(b) shows the corresponding δE_z vs. $V_A \delta B_y$ during the interval from $t = 0.0$ to $t = 80.0$. Three stages are identified from Figure 5(a). In the stage from $t = 0$ to about $t = 27.0$, the disturbances are of small amplitude, with no apparent relationship between the perturbations of electric field and magnetic field. Strong wave perturbations then appear about
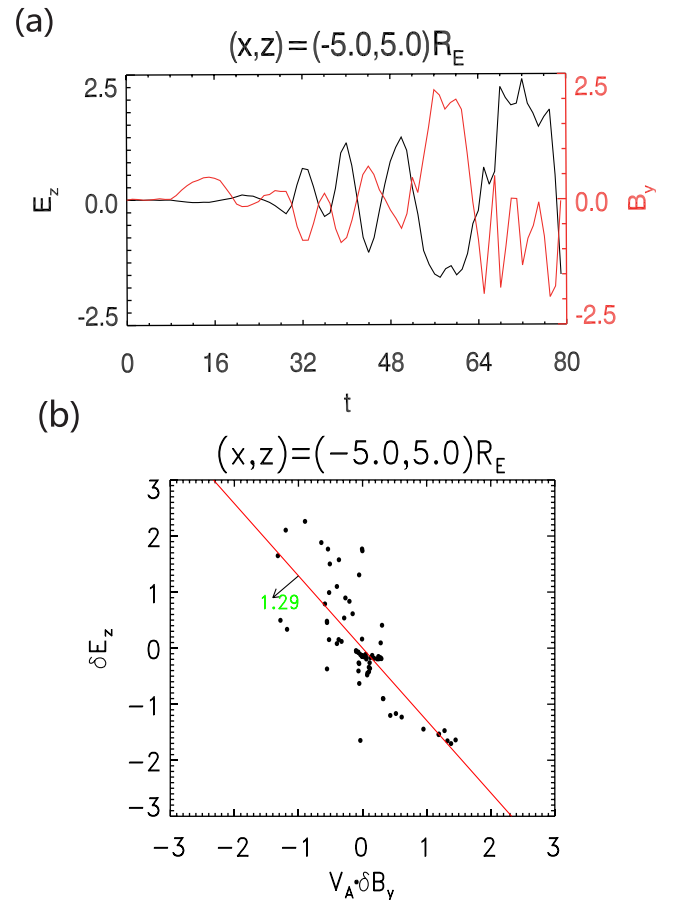

FIG. 5. (a) Contour plots of the time evolution of the electric field E_z (black line) and the magnetic field B_y (red line) at $(x, z) = (-5.0, 5.0)R_E$. (b) The corresponding δE_z vs. $V_A \delta B_y$ during the interval from $t = 0.0$ to $t = 80.0$. The solid line shows the fitted value (-1.29) based on the simulation data.

$t = 27.0$. In the stage from $t = 27.0$ to t $= 54.0$, coherent perturbations are seen between B_y and E_z, with a nearly $180°$ phase difference in Figure 5(a). After $t = 54.0$, the perturbations show a more complicated structure due to the arrival of reflected waves from the ionospheric boundary, and the amplitudes become larger. Overall, the ratio $\delta E_z / \delta B_y$ is nearly equal to $-1.29 V_A$, which is based on the simulation data and shown by the red solid line in Figure 5(b). This ratio agrees well with that based on the dispersion relation of KAWs.[17,51–53] Therefore, the polarization relation obtained from the simulation agrees very well with the theoretical prediction and dispersion relation of KAWs.

In the regions with KAWs or shear Alfven waves, the ion velocity distribution evolves significantly with time. Figure 6(a) shows contour plots of the ion velocity distributions in the $v_x - v_z$ plane (left column) and the $v_x - v_y$ plane (right column) for times t $= 0.0$ (top row), 44.0 (middle row),

and 60.0 (bottom row), for the high-latitude region at $(x, z) = (-5.0, 4.0) R_E$ of region "c." The white arrows in Figure 6 show the direction of the local magnetic field. Initially, the ion distribution is nearly isotropic with a nearly zero bulk velocity. At $t = 44.0$, the distribution has become a triple-humped structure, with an ion beam centered at $(v_x, v_y, v_z) \approx (0.35, 0, 0)$ along the magnetic field (nearly points to the x direction in this high-latitude region) and another ion beam centered at $(v_x, v_y, v_z) \approx (-0.35, 0, 0)$ opposite to the magnetic field, in addition to the core plasma population. At $t = 60.0$, the distribution exhibits a single, heated component, with a larger perpendicular than parallel temperature. Figure 6(b) plots the results at $(x, z) = (-10.0, 0.0) R_E$ down tail in the low-latitude of region "a." At $t = 0$, the ion velocity distribution is almost isotropic, without a bulk velocity. At $t = 44.0$, the distribution has become a double-humped structure, with an ion component
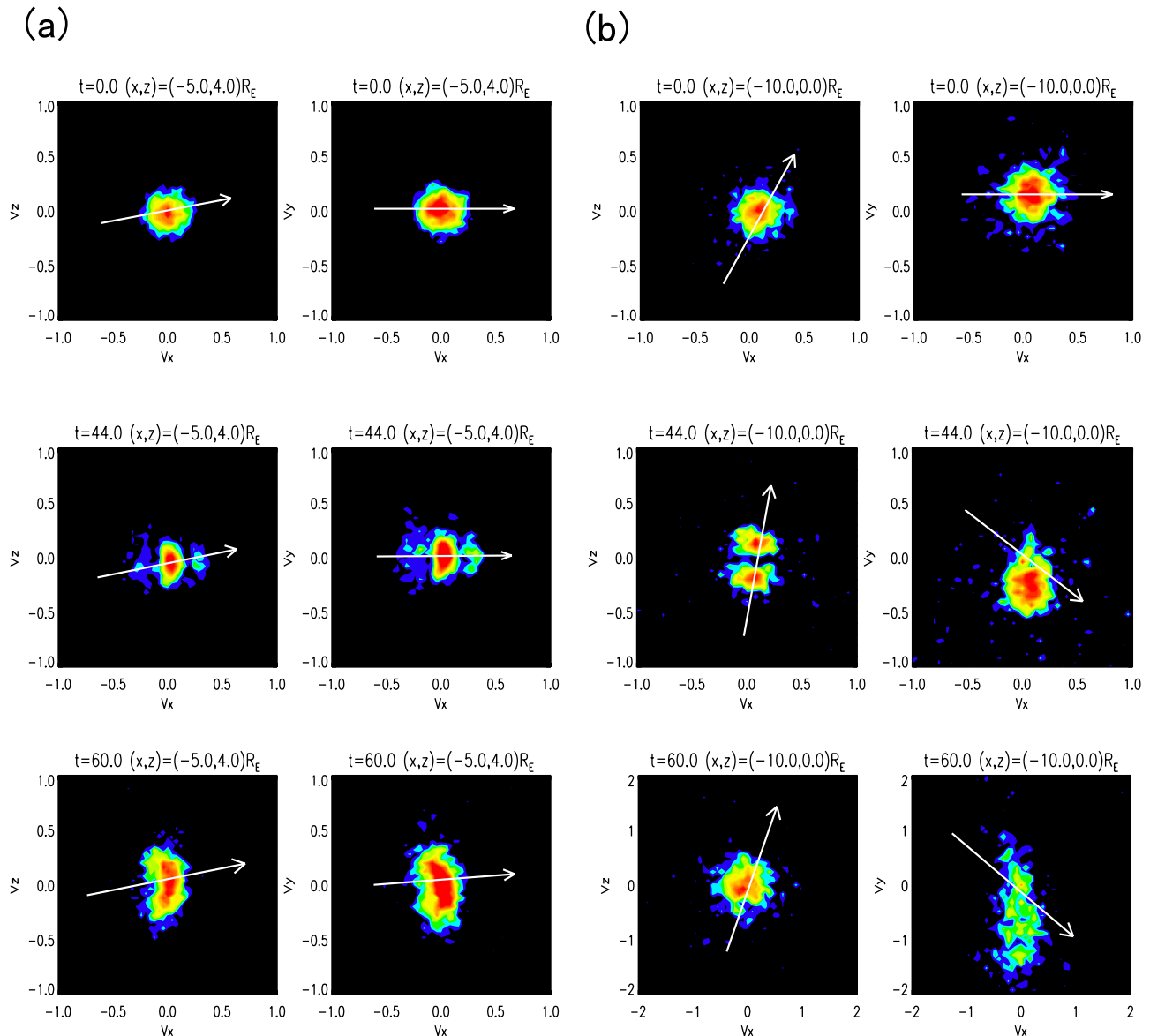
(a)   (b)

FIG. 6. (a) The ion velocity distributions in the high-latitude region at $(x, z) = (-5.0, 4.0) R_E$ of region "c" in the $v_x - v_z$ plane (left column) and the $v_x - v_y$ plane (right column) for times t $= 0.0$ (top row), 44.0 (middle row), and 60.0 (bottom row). (b) Ion velocity distributions at $(x, z) = (-10.0, 0.0) R_E$ in the low-latitude downtail of region "a" at times $t = 0.0$, 44.0, and 60.0. The white arrows show the direction of the local magnetic field.

$v_z \sim 0.2$ along the magnetic field (almost pointing to the z direction in this low-latitude magnetotail) and another ion component $v_z \sim -0.2$ opposite to the magnetic field. Note that since the location for Figure 6(b) is just earthward of the flow braking, no large ion velocity is observed in the v_x direction. At $t = 60.0$, the distribution exhibits a larger perpendicular than parallel temperature. These results are consistent with the results of Hong, Swift, and Lin.[47]

IV. SUMMARY AND DISCUSSION

In this paper, we have carried out a 2-D global hybrid simulation to investigate the evolution of Alfven waves in the magnetotail. The fast Earthward flow is initiated by the $\boldsymbol{E} \times \boldsymbol{B}$ drift, which then leads to the plasma sheet thinning and a dipolarization of the tail magnetic field. When the earthward flow reaches the strong dipole field region, it is braked by the geomagnetic field, and the ion flow has a significant northward and southward diversion. Subsequently, the dipolarization spreads tailward, and the tailward flows appear. These simulation results are in good agreement with observations, which show the occurrence of the tailward flow increases during the magnetotail stretching, and the flow decreases or ceases during magnetic field dipolarization.[48] When the fast flow encounters the stationary near-Earth plasma, low-frequency shear Alfven waves are generated. The Alfven waves are identified by analyzing the dispersion relation of the wave modes for the fluctuations in the low-latitude magnetotail. These Alfven waves propagate towards the polar regions along the magnetic field lines, and evolve into kinetic Alfven waves in the high-latitude magnetosphere, where the magnetic field and density are non-uniform. The KAWs are identified by analyzing the dispersion relation, perpendicular wavelength, and the polarization relation between magnetic and electric fields. Our simulation gives an explanation for the source of the observed kinetic Alfven waves in the high-latitude of the near-Earth magnetotail. In the satellite observation by Wygant *et al.*,[17] it was also speculated that the kinetic Alfven waves above the auroral acceleration region at altitudes of $4R_E - 7R_E$ of the plasma sheet may be originated from the shear Alfven waves in the low-latitudes.

The process of the conversion of kinetic Alfven waves from shear Alfven waves in a non-uniform magnetic field and density has been studied in Ref. 29. Our simulation suggests that the KAWs in the high-latitude magnetotail are generated from the shear Alfven waves in the low-latitudes through mechanism similar process. The shear Alfven waves are generated by the interaction of the fast earthward flow with the stationary near-Earth plasma around $(x, z) = (-10.0, 0.0)R_E$. These Alfven waves propagate towards the polar regions along the magnetic field lines. Due to the existence of the non-uniform background, the spatial variation of the local Alfven speed leads to an inclination of the wave front. The perpendicular wave number k_z becomes dominant through a phase mixing process. In our simulation, the shear Alfven waves are found to evolve into kinetic Alfven waves with a large $k_\perp$ in the high-latitude polar regions.

Many researchers have proposed that auroral electrons are produced when a field-aligned electric field is developed within KAWs.[1,9,11,54,55] In particular, the physical nature in the auroral ionosphere and magnetosphere can be well explained by *in situ* observations of KAWs with the polar orbiting satellites, Freja, FAST, Cluster.[18,19,52,56–61] Both *in situ* measurements and numerical simulation investigations provide further evidence that KAWs can be responsible for the field-aligned energization of electrons that drive bright aurora.[51,62–64]

KAWs are dissipative as well as dispersive waves because their perpendicular wavelengths have scales comparable to the microscopic kinetic scales of particles, such as the ion gyroradius or the electron inertial length. The focus of this study is on the KAWs whose perpendicular wavelengths are comparable to the ion gyroradius. Due to the assumption of the massless electron, the electron-scale physics of KAWs is not addressed in our hybrid model. Another limitation of the model is that in the 2-D assumption, effects of the east-west diversion of the plasma are not included. Previous simulations have shown that the generation of KAWs may be dominated by the 2-D physics,[21,29] however, further 3-D studies are necessary to understand the fully nonlinear evolution of KAWs.[22]

Energies of the distant magnetotail can be transported into the near-Earth magnetotail through the fast earthward flow. Our simulation shows that Alfven waves are generated by the interaction of the fast flow with the stationary near-Earth plasma, and turbulence energy is then radiated away from the equatorial region as Alfven waves propagate towards the polar regions. It has been found that the turbulent cascade process of shear Alfven waves to small-scale KAWs, and the associated wave-particle interaction can lead to the energy conversion from waves to the particles since the scale lengths of KAWs match the particle kinetic scales by previous studies. The particles can be effectively accelerated in this way. Such process may play an important role in the auroral particle acceleration. So the generation of shear Alfven waves and KAWs shown in our simulation may also provide a process for the energy transport from the distant magnetotail to near-Earth magnetosphere. Nevertheless, while the spectrum of kinetic Alfven waves observed by spacecraft is usually of a broadband, our present simulation has only run to a limited duration corresponding to the tail convection time scales, and thus the broadband spectrum has not been fully developed. A longer simulation is required in order to investigate the fully developed turbulence spectrum.

[1]A. Hasegawa, J. Geophys. Res. **81**(28), 5083–5090, doi:10.1029/JA081i028p05083 (1976).

[2]R. L. Lysak and W. Lotko, J. Geophys. Res. **101**(A3), 5085–5094, doi:10.1029/95JA03712 (1996).

[3]D. J. Wu, Phys. Plasmas **10**, 1364 (2003).

[4]R. L. Lysak, Geophys. Res. Lett. **25**, 2089, doi:10.1029/98GL00065 (1998).

[5]A. Hasegawa and L. Chen, Phys. Rev. Lett. **35**, 370 (1975).

[6]A. Hasegawa and L. Chen, Phys. Fluids **19**, 1924 (1976).

[7]D. W. Ross, G. L. Chen, and S. M. Mahajan, Phys. Fluids **25**, 652 (1982).

[8]R. L. Lysak and C. T. Dum, J. Geophys. Res. **88**(A1), 365–380, doi:10.1029/JA088iA01p00365 (1983).

[9]C. K. Goertz, Planet. Space Sci. **32**, 1387 (1984).

[10]D. J. Wu and J. K. Chao, J. Geophys. Res. **109**, A06211, doi:10.1029/2003JA010126 (2004).

[11]L. C. Lee, J. R. Johnson, and Z. W. Ma, J. Geophys. Res. **99**(A9), 17405–17411, doi:10.1029/94JA01095 (1994).

[12]Y. V. Oitenko and M. Goossens, Astrophys. J. **605**, L149–L152 (2004).

[13]D. J. Wu and L. Yang, Astron. Astrophys. **452**, L7–L10 (2006).

[14]C. Chaston, J. Bonnell, J. P. McFadden, C. W. Carlson, C. Cully, O. Le Contel, A. Roux, H. U. Auster, K. H. Glassmeier, V. Angelopoulos, and C. T. Russell, Geophys. Res. Lett. **35**, L17S08, doi:10.1029/2008GL033601 (2008).

[15]R. L. Lysak and Y. Song, J. Geophys. Res. **108**, 8005, doi:10.1029/2002JA009406 (2003).

[16]C. C. Chaston, C. W. Carlson, J. P. McFadden, R. E. Ergun, and R. J. Strangeway, Geophys. Res. Lett. **34**, L07101, doi:10.1029/2006GL029144 (2007).

[17]J. R. Wygant, A. Keiling, C. A. Cattell, R. L. Lysak, M. Temerin, F. S. Mozer, C. A. Kletzing, J. D. Scudder, V. Streltsov, W. Lotko, and C. T. Russell, J. Geophys. Res. **107**(A8), 1201, doi:10.1029/2001JA900113 (2002).

[18]J. Dombeck, C. Cattell, J. R. Wygant, A. Keiling, and J. Scudder, J. Geophys. Res. **110**, A12S90, doi:10.1029/2005JA011269 (2005).

[19]A. Keiling, J. R. Wygant, C. Cattell, W. Peria, G. Parks, M. Temerin, F. S. Mozer, C. T. Russell, and C. A. Kletzing, J. Geophys. Res. **107**(A7), 1132, doi:10.1029/2001JA900140 (2002).

[20]M. Tanaka, T. Sato, and A. Hasegawa, Phys. Fluids B **1**, 325–332 (1989).

[21]Y. Lin, J. R. Johnson, and X. Y. Wang, J. Geophys. Res. **115**, A04208, doi:10.1029/2009JA014524 (2010).

[22]Y. Lin, J. R. Johnson, and X. Y. Wang, Phys. Rev. Lett. **109**, 125003 (2012).

[23]H. Grad, Proc. Natl. Acad. Sci. U.S.A. **70**, 3277 (1973).

[24]A. Hasegawa and L. Chen, Phys. Rev. Lett. **32**, 454–456 (1974).

[25]L. Chen and A. Hasegawa, J. Geophys. Res. **79**(7), 1024–1032, doi:10.1029/JA079i007p01024 (1974).

[26]B. V. Tiwari, R. Mishra, P. Varma, and M. S. Tiwari, Indian J. Pure Appl. Phys. **44**, 917–926 (2006), see http://nopr.niscair.res.in/handle/123456789/8387.

[27]B. V. Tiwari, R. Mishra, P. Varma, and M. S. Tiwari, Earth Planets Space **60**, 191–205 (2008).

[28]A. Jaun, K. Appert, A. Fasoli, T. Hellsten, J. Vaclavik, and L. Villard, Plasma Phys. Controlled Fusion **39**, 549 (1997).

[29]M. H. Hong, Y. Lin, and X. Y. Wang, Phys. Plasmas **19**, 072903 (2012).

[30]V. Angelopoulos, W. Baumjohann, C. F. Kennel, F. V. Coroniti, M. G. Kivelson, R. Pellat, R. J. Walker, H. Lühr, and G. Paschmann, J. Geophys. Res. **97**(A4), 4027–4039, doi:10.1029/91JA02701 (1992).

[31]T. Nagai, M. Fujimoto, Y. Saito, S. Machida, T. Terasawa, R. Nakamura, T. Yamamoto, T. Mukai, A. Nishida, and S. Kokubun, J. Geophys. Res. **103**(A3), 4419–4440, doi:10.1029/97JA02190 (1998).

[32]S. Machida, Y. Miyashita, A. Ieda, A. Nishida, T. Mukai, Y. Saito, and S. Kokubun, Geophys. Res. Lett. **26**(6), 635–638, doi:10.1029/1999GL900030 (1999).

[33]K. Kondoh and M. Ugai, Adv. Space Res. **39**, 1378–1381 (2007).

[34]Y. Miyashita, S. Machida, Y. Kamide, D. Nagata, K. Liou, M. Fujimoto, A. Ieda, M. H. Saito, C. T. Russell, S. P. Christon, M. Nosé, H. U. Frey, I. Shinohara, T. Mukai, Y. Saito, and H. Hayakawa, J. Geophys. Res. **114**, A01211, doi:10.1029/2008JA013225 (2009).

[35]Y. Miyashita, S. Machida, A. Ieda, D. Nagata, Y. Kamide, M. Nosé, K. Liou, T. Mukai, S. P. Christon, C. T. Russell, I. Shinohara, and Y. Saito, J. Geophys. Res. **115**, A12239, doi:10.1029/2010JA015608 (2010).

[36]V. Angelopoulos, T. D. Phan, D. E. Larson, F. S. Mozer, R. P. Lin, K. Tsuruda, H. Hayakawa, T. Mukai, S. Kokubun, T. Yamamoto, D. J.

Williams, R. W. McEntire, R. P. Lepping, G. K. Parks, M. Brittnacher, G. Germany, J. Spann, H. J. Singer, and K. Yumoto, Geophys. Res. Lett. **24**, 2271–2274, doi:10.1029/97GL02355 (1997).

[37]R. Nakamura, W. Baumjohann, C. Mouikis, L. M. Kistler, A. Runov, M. Volwerk, Y. Asano, Z. Vörös, T. L. Zhang, B. Klecker, H. Rème, and A. Balogh, Geophys. Res. Lett. **31**, L09804, doi:10.1029/2004GL019558 (2004).

[38]V. A. Sergeev, J. A. Sauvaud, K. Popescu, R. A. Kovrazhkin, K. Liou, P. T. Newell, M. Brittnacher, G. Parks, R. Nakamura, T. Mukai, and G. D. Reeves, Geophys. Res. Lett. **27**, 851, doi:10.1029/1999GL010729 (2000).

[39]M. Ugai, K. Kondoh, and T. Shimizu, Phys. Plasmas **10**, 357 (2003).

[40]K. Shiokawa, W. Baumjohann, and G. Haerendel, Geophys. Res. Lett. **24**, 1179–1182, doi:10.1029/97GL01062 (1997).

[41]M. Hesse, D. Winske, and M. Kuznetsova, J. Geophys. Res. **100**, 21815–21826, doi:10.1029/95JA01559 (1995).

[42]D. Krauss-Vargan and N. Omidi, Geophys. Res. Lett. **22**, 3271, doi:10.1029/95GL03414 (1995).

[43]Y. Lin and D. W. Swift, J. Geophys. Res. **101**, 19859–19870, doi:10.1029/96JA01457 (1996).

[44]H. Karimabadi, D. Krauss-Varban, J. D. Huba, and H. X. Vu, J. Geophys. Res. **109**, A09205, doi:10.1029/2004JA010478 (2004).

[45]Y. Lin and D. W. Swift, J. Geophys. Res. **107**(A11), 1373, doi:10.1029/2002JA009308 (2002).

[46]D. W. Swift and Y. Lin, J. Atmos. Sol.-Terr. Phys. **63**, 683–704 (2001).

[47]M. H. Hong, D. W. Swift, and Y. Lin, Adv. Space Res. **41**, 1298–1304 (2008).

[48]A. M. Du, R. Nakamura, T. L. Zhang, E. V. Panov, W. Baumjohann, H. Luo, W. Y. Xu, Q. M. Lu, M. Volwerk, A. Retinò, B. Zieger, V. Anglopoulos, K.-H. Glassmeier, J. P. McFadden, and D. Larson, J. Geophys. Res. **116**, A03216, doi:10.1029/2010JA015969 (2011).

[49]J. V. Hollweg, J. Geophys. Res. **104**(A7), 14811–14819, doi:10.1029/1998JA900132 (1999).

[50]R. J. Leamon, C. W. Smith, N. F. Ness, and H. K. Wong, J. Geophys. Res. **104**(A10), 22331–22344, doi:10.1029/1999JA900158 (1999).

[51]K. Stasiewicz, P. Bellan, C. Chaston, C. Kletzing, R. Lysak, J. Maggs, O. Pokhotelov, C. Seyler, P. Shukla, L. Stenflo, A. Streltsov, and J.-E. Wahlund, Space Sci. Rev. **92**(3–4), 423–533 (2000).

[52]M. Volwerk, P. Louarn, T. Chust, A. Roux, H. deFeraudy, and B. Holback, J. Geophys. Res. **101**(A6), 13335–13343, doi:10.1029/96JA00166 (1996).

[53]A. Keiling, Space Sci. Rev. **142**(1–4), 73–156 (2009).

[54]C. K. Goertz and R. W. Boswell, J. Geophys. Res. **84**(A12), 7239–7246, doi:10.1029/JA084iA12p07239 (1979).

[55]C.-H. Hui and C. E. Seyler, J. Geophys. Res. **97**(A4), 3953–3963, doi:10.1029/91JA03101 (1992).

[56]P. Louarn, J. E. Wahlund, T. Chust, H. de Feraudy, A. Roux, B. Holback, P. O. Dovner, A. I. Eriksson, and G. Holmgren, Geophys. Res. Lett. **21**, 1847–1850, doi:10.1029/94GL00882 (1994).

[57]J.-E. Wahlund, P. Louarn, T. Chust, H. de Feraudy, A. Roux, B. Holback, P. Dovner, and G. Holmgren, Geophys. Res. Lett. **21**, 1831–1834, doi:10.1029/94GL01289 (1994).

[58]K. Stasiewicz, Y. Khotyaintsev, M. Berthomier, and J.-E. Wahlund, Geophys. Res. Lett. **27**, 173–176, doi:10.1029/1999GL010696 (2000).

[59]C. C. Chaston, C. W. Carlson, W. J. Peria, R. E. Ergun, and J. P. McFadden, Geophys. Res. Lett. **26**, 647, doi:10.1029/1998GL900246 (1999).

[60]A. Keiling, J. R. Wygant, C. Cattell, M. Johnson, M. Temerin, F. S. Mozer, C. A. Kletzing, J. Scudder, and C. T. Russell, J. Geophys. Res. **106**(A4), 5779–5798, doi:10.1029/2000JA900130 (2001).

[61]T. Wang, J. Cao, H. Fu, W. Liu, and M. Dunlop, J. Geophys. Res. **119**, 9527–9542, doi:10.1002/2014JA019997 (2014).

[62]C. C. Chaston, J. W. Bonnell, C. W. Carlson, J. P. McFadden, R. E. Ergun, and R. J. Strangeway, J. Geophys. Res. **108**, 8003, doi:10.1029/2002JA009420 (2003).

[63]C. C. Chaston, J. W. Bonnell, C. W. Carlson, J. P. McFadden, R. E. Ergun, R. J. Strangeway, and E. J. Lund, J. Geophys. Res. **109**, A04205, doi:10.1029/2003JA010053 (2004).

[64]C. C. Chaston, L. M. Peticolas, C. W. Carlson, J. P. McFadden, F. Mozer, M. Wilber, G. K. Parks, A. Hull, R. E. Ergun, R. J. Strangeway, M. Andre, Y. Khotyaintsev, M. L. Goldstein, M. Acuña, E. J. Lund, H. Reme, I. Dandouras, A. N. Fazakerley, and A. Balogh, J. Geophys. Res. **110**, A02211, doi:10.1029/2004JA010483 (2005).